

Comparing the spatial structure of variability in two datasets against each other on the basis of EOF-modes

Tobias Bayr · Dietmar Dommenges

Received: 13 November 2012 / Accepted: 18 February 2013 / Published online: 12 March 2013
© Springer-Verlag Berlin Heidelberg 2013

Abstract In analysis of climate variability or change it is often of interest how the spatial structure in modes of variability in two datasets differ from each other, e.g. between past and future climate or between models and observations. Often such analysis is based on Empirical Orthogonal Function (EOF) analysis or other simple indices of large-scale spatial structures. The present analysis lays out a concept on how two datasets of multivariate climate variability can be compared against each other on basis of EOF analysis and how the differences in the multivariate spatial structure between the two datasets can be quantified in terms of explained variance in the leading spatial patterns. It is also illustrated how the patterns of largest differences between the two datasets can be defined and interpreted. We illustrate this method on the basis of several well-defined artificial examples and by comparing our approach with examples of climate change studies from the literature. These literature examples include analysis of changes in the modes of variability under climate change for the sea level pressure (SLP) of the North Atlantic and Europe, the SLP of the Southern Hemisphere, the surface temperature of the Northern Hemisphere, the sea surface temperature of the North Pacific and for precipitation in the tropical Indo-Pacific.

Electronic supplementary material The online version of this article (doi:10.1007/s00382-013-1708-x) contains supplementary material, which is available to authorized users.

T. Bayr (✉)
GEOMAR Helmholtz Centre for Ocean Research,
Düsternbrooker Weg 20, 24105 Kiel, Germany
e-mail: tbayr@geomar.de

D. Dommenges
School of Mathematical Sciences, Monash University,
Clayton, VIC, Australia

Keywords Modes of variability · Spatial structure of variability · Empirical orthogonal functions · Global warming

1 Introduction

Climate variability has significant spatial structure that is often characterized by so called modes of variability. Such modes are, for instance, the El Niño Southern Oscillation (ENSO), the Pacific Decadal Oscillation (PDO), the North Atlantic Oscillation (NAO) or the Southern Annular Mode (SAM). These modes are assumed to be quasi-fixed spatial patterns (Wallace and Gutzler 1981), that represent a relative large part of climate variability. Alternatively one can think of the climate variability as a multivariate stochastic process, which has a continuum of spatial patterns of variability (e.g. see discussion in Dommenges 2007; hereafter D07). Independent of whether we think of the climate variability as fixed modes (factors) or a continuum of spatial patterns reflecting a multivariate stochastic process, often the question arises: What are the differences in the spatial structures of variability between one time period and another or between a control and a sensitivity experiment or between model simulations and observations? The aim of this study presented here is to outline a concept of how such a comparison can be done in a quantitative way on the basis of Empirical Orthogonal Function (EOF) analysis (also known as principal component analysis).

As the multivariate structure of any dataset is unique and different from any other dataset, a special frame is needed to be able to compare the multivariate structure of two data sets. Jolliffe (2002, Chapter 13.5) gives a nice overview about EOF related technics for comparing the multivariate structure in two or more datasets against each other. Some of these technics aim to find some common eigenvectors, which are

then used as basis to compare the individual datasets (e.g. in common principal component analysis in Sengupta and Boyle 1998). Some other technics suggest a criterion like the angle between the eigenvectors of different datasets to find out if eigenvectors differ significantly from each other (e.g. in Krzanowski 1979). Beyond that several other technics were used in recent literature to investigate the changes in the modes of variability under increased greenhouse gas emissions (e.g. Osborn 2004; Rauthe et al. 2004; Hu and Wu 2004; Kuzmina 2005; McHugh and Rogers 2005; Miller et al. 2006; Stephenson et al. 2006; Keeley et al. 2008). Most of these technics focus on the changes in one particular mode or compare the leading modes pairwise. Although this gives a good discussion of how the particular investigated leading modes will change, it remains unclear whether this change is representative for the whole multivariate stochastic variability or it is the most important change in the dataset. Considering only the dominant mode in the dataset will in most cases exclude the largest part of the variability that is represented by all the other modes of variability. It also needs to be considered that the changes in the spatial structure of the variability may not be well described by the changes in one or two particular modes at all. The change in the spatial structure of variability is not limited to intensification, reduction or shift in one pattern, but it could, for instance, be a change in the length scale of variability in general, a change in the higher ordered modes or a change of in multiple patterns, thus of the multivariate structure.

The method that we will describe is based on the Distinct Empirical Orthogonal Function (DEOF) analysis introduced by D07. The basic idea is similar to the one of Krzanowski (1979), but our method takes the whole multivariate structure of the two datasets into account. The method allows to objectively quantify differences between the multivariate structure of two datasets and it allows to define the patterns which best describe these differences. The paper is organised as follows: In Sect. 2 the data used in this study are presented, and the new method is introduced in Sect. 3. The statistical significance levels of the DEOF patterns are discussed in Sect. 4. How this method works and how the results can be interpreted is illustrated in Sect. 5 on the basis of four well-defined constructed examples. The robustness of this method is then compared against several literature examples of studies about changes in the modes of variability under climate change scenarios in Sect. 6. The study is concluded with Sect. 7.

2 Data

The data analysed in this study are taken from the Climate Model Intercomparison Project 3 (CMIP3, Meehl et al. 2007). We selected all climate models, which had sea level pressure (SLP), surface temperature (T_{surf}), sea surface temperature

Table 1 List of climate models taken from the CMIP3 database

Model	Institute
BCCR-BCM2.0	Bjerknes Centre for Climate Research, Norway
CGCM3.1(T63)	Canadian Centre for Climate Modelling and Analysis, Canada
CGCM3.1(T47)	Canadian Centre for Climate Modelling and Analysis, Canada
CNRM-CM3	Centre National de Recherches Meteorologiques, France
CSIRO-Mk3.0	Commonwealth Scientific and Industrial Research Organisation, Australia
CSIRO-Mk3.5	Commonwealth Scientific and Industrial Research Organisation, Australia
GFDL-CM2.0	Geophysical Fluid Dynamics Laboratory, USA
GFDL-CM2.1	Geophysical Fluid Dynamics Laboratory, USA
GISS-AOM	Goddard Institute for Space Studies, USA
GISS-EH	Goddard Institute for Space Studies, USA
GISS-ER	Goddard Institute for Space Studies, USA
IAP-FGOALS-g1.0	Institute of Atmospheric Physics, China
INGV-SXG	Italian National Institute of Geophysics and Volcanology, Italy
INM-CM3.0	Institute for Numerical Mathematics, Russia
IPSL-CM4	Institut Pierre Simon Laplace, France
MIROC3.2(hires)	Center for Climate System Research, Japan
MIROC3.2(medres)	Center for Climate System Research, Japan
MIUB-ECHO-G	Meteorological Institute of the University of Bonn, Meteorological Research Institute of the Korea, Germany/Korea
MPI-ECHAM5	Max Planck Institute for Meteorology, Germany
MRI-CGCM2.3.2	Meteorological Research Institute, Japan
NCAR-CCSM3	National Center for Atmospheric Research, USA
NCAR-PCM	National Center for Atmospheric Research, USA
UKMO-HadCM3	Hadley Centre for Climate Prediction and Research/Met Office, UK
UKMO-HadGEM1	Hadley Centre for Climate Prediction and Research/Met Office, UK

(SST) and precipitation available for the present day (20C) and global warming scenario (A1B); see Table 1 for a list of climate models. For each model simulation the linear trend and mean annual cycle is subtracted to define anomalies which are interpolated onto a common $2.5^\circ \times 2.5^\circ$ grid. The anomalies of the 24 individual model simulations are then concatenated to build one multi model ensemble dataset with one ensemble member from each model.

3 Method of comparing two sets of EOF-modes

In the following we assume that the spatial structure of the variability in two datasets is well represented by the

leading EOF-modes of each dataset. Note that the set of EOF-modes of any dataset is unique and different from any other dataset. In order to be able to compare the relative importance of the different modes in two different datasets we need to define a common reference set of modes. A method of comparing two sets of EOF-modes against each other has been discussed in D07. Therein the EOF-modes of a dataset are compared against the EOF-modes of the stochastic null hypothesis of isotropic diffusion by projecting the leading EOF-modes of the isotropic diffusion process onto the EOF-modes of the dataset. This approach can be generalized by replacing the EOF-modes of the stochastic null hypothesis with the EOF-modes of any other dataset. Thus we define the EOF-modes of our first dataset “ \mathcal{A} ” as the reference modes. The variance that each (i -index) of the reference modes from dataset \mathcal{A} , $\vec{E}_i^{\mathcal{A}}$ would explain in the dataset \mathcal{B} can be estimated by projecting all of the EOF patterns of \mathcal{A} , $\vec{E}_i^{\mathcal{A}}$, onto the EOF pattern of \mathcal{B} , $\vec{E}_j^{\mathcal{B}}$, or in shortened form, $\mathcal{A} \rightarrow \mathcal{B}$. Due to the orthogonality of the EOF pattern, the sum over all linear combinations gives us the explained variance the EOF pattern of $\vec{E}_i^{\mathcal{A}}$ would have in the dataset \mathcal{B} :

$$pev_i^{\mathcal{A} \rightarrow \mathcal{B}} = \sum_{j=1}^N c_{ij}^2 ev_j^{\mathcal{B}} \tag{1}$$

with projected explained variance, $pev_i^{\mathcal{A} \rightarrow \mathcal{B}}$, the explained variance of the j th EOF pattern in dataset \mathcal{B} , $ev_j^{\mathcal{B}}$ and

$$c_{ij} = \frac{\vec{E}_j^{\mathcal{B}} \vec{E}_i^{\mathcal{A}}}{|\vec{E}_j^{\mathcal{B}}| |\vec{E}_i^{\mathcal{A}}|} \quad (\text{pattern correlation}) \tag{2}$$

It is important to note that the projected explained variances $pev_i^{\mathcal{A} \rightarrow \mathcal{B}}$ do not have to be monotonically decreasing as the explained variances of EOF-modes do. An EOF-mode that explains at lot of variance in dataset \mathcal{A} does not need to explain as much variance in dataset \mathcal{B} and vice versa. We can now directly compare the spectrum of $ev_i^{\mathcal{A}}$ values against the $pev_i^{\mathcal{A} \rightarrow \mathcal{B}}$ values to estimate which modes have different strength in the two datasets.

One has to keep in mind that the differences between the two datasets may be largest in a pattern that does not project well onto any of the EOF-modes. In order to find the pattern which shows the largest differences in explained variance between the two datasets it is necessary to rotate the EOF-modes to a set of patterns that maximize the difference in explained variance between the two datasets. These modes are called the DEOF patterns. They can be found by pairwise rotation of the EOF-modes to maximize the difference in the leading $ev_i^{\mathcal{A}}$ values relative to the $pev_i^{\mathcal{A} \rightarrow \mathcal{B}}$ (See D07 for details).

The DEOF patterns have two explained variance values: one is corresponding to the amount of variance the pattern explains in dataset \mathcal{A} , $dev^{\mathcal{A} \rightarrow \mathcal{B}}(\mathcal{A})$, and the other is the corresponding values for dataset \mathcal{B} , $dev^{\mathcal{A} \rightarrow \mathcal{B}}(\mathcal{B})$. The DEOF-modes are ordered by the difference in explained variance between $dev^{\mathcal{A} \rightarrow \mathcal{B}}(\mathcal{A})$ and $dev^{\mathcal{A} \rightarrow \mathcal{B}}(\mathcal{B})$, and not, as in EOF analysis, by the explained variance of the pattern. It is important to keep in mind that interpretation of the DEOF-patterns can be equally difficult as for the normal EOF-modes.

The leading DEOF-mode, DEOF-1 $^{\mathcal{A} \rightarrow \mathcal{B}}$, is the pattern that explains more variance in dataset \mathcal{A} than in dataset \mathcal{B} . No other pattern can have a larger difference in the explained variance between the two datasets, $\Delta dev^{\mathcal{A} \rightarrow \mathcal{B}} = dev^{\mathcal{A} \rightarrow \mathcal{B}}(\mathcal{A}) - dev^{\mathcal{A} \rightarrow \mathcal{B}}(\mathcal{B})$, than DEOF-1, as the pattern are ordered by their $\Delta dev^{\mathcal{A} \rightarrow \mathcal{B}}$. In turn, if we want to know which patterns have a higher explained variance in dataset \mathcal{B} than in dataset \mathcal{A} , we have to repeat the analysis by defining the EOF-modes of dataset \mathcal{B} as our reference modes and project the EOF-modes of dataset \mathcal{B} onto the EOF-modes of dataset \mathcal{A} (DEOF $^{\mathcal{B} \rightarrow \mathcal{A}}$). A MATLAB-script that does the complete analysis is provided as a supplementary material and the nomenclature used in this paper is summed up in Table 2.

4 Uncertainties of DEOF-modes

In the discussion of the DEOF-modes it is important to know whether the difference $\Delta dev^{\mathcal{A} \rightarrow \mathcal{B}}$ is just a reflection of sampling uncertainties or whether it is an indication of differences in the stochastic processes underlying the two datasets. Thus we need to know the probability density function (*pdf*) of Δdev under the null hypothesis that the stochastic processes in the two datasets are the same (sampling uncertainty).

The rule of thumb for EOF analysis from North et al. (1982) gives the sampling uncertainty range of an

Table 2 Nomenclature for terms in EOF and DEOF analysis

EOF analysis	
EOF pattern of data set \mathcal{A}	$\vec{E}_i^{\mathcal{A}}$
EOF pattern of data set \mathcal{B}	$\vec{E}_j^{\mathcal{B}}$
Explained variances of EOF pattern of \mathcal{A}	$ev_i^{\mathcal{A}}$
DEOF analysis	
Explained variance of $\vec{E}_i^{\mathcal{A}}$ projected on \mathcal{B}	$pev_i^{\mathcal{A} \rightarrow \mathcal{B}}$
DEOF pattern from projection of \mathcal{A} on \mathcal{B}	DEOF- $i^{\mathcal{A} \rightarrow \mathcal{B}}$
Explained variance of DEOF- $i^{\mathcal{A} \rightarrow \mathcal{B}}$ in data set \mathcal{A}	$dev_i^{\mathcal{A} \rightarrow \mathcal{B}}(\mathcal{A})$
Explained variance of DEOF- $i^{\mathcal{A} \rightarrow \mathcal{B}}$ in data set \mathcal{B}	$dev_i^{\mathcal{A} \rightarrow \mathcal{B}}(\mathcal{B})$
Difference $dev_i^{\mathcal{A} \rightarrow \mathcal{B}}(\mathcal{A}) - dev_i^{\mathcal{A} \rightarrow \mathcal{B}}(\mathcal{B})$	$\Delta dev_i^{\mathcal{A} \rightarrow \mathcal{B}}$

eigenvalue, which is essentially the standard deviation of the *pdf* of the eigenvalue. For the DEOF analysis we have to estimate the expectation value of the difference $\Delta dev^{A \rightarrow B} = dev^{A \rightarrow B}(\mathcal{A}) - dev^{A \rightarrow B}(\mathcal{B})$ as well as the spread around it. To estimate the *pdf* of DEOF analysis we followed a bootstrapping approach: As the stochastic process we chose isotropic diffusion, as it is a useful null hypothesis for climate variability and has a well-defined structure of multi-poles in the EOF-modes (for details see D07). It can be described for any space and time dependent variable $\Phi(\vec{x}, t)$ with the following differential equation:

$$\frac{d}{dt} \Phi(\vec{x}, t) = c_{damp} \cdot \Phi(\vec{x}, t) + c_{diffuse} \cdot \nabla^2 \Phi(\vec{x}, t) + f(\vec{x}, t) \quad (3)$$

where $c_{damp} < 0$ is a constant for local linear damping, $c_{diffuse}$ is the diffusion coefficient and $f(\vec{x}, t)$ is spatial and temporal white noise forcing. First, we generated a large ensemble of isotropic diffusion processes (Eq. 3) with different white noise realizations, the same spatial number degrees of freedom $N_{spatial}$ (Bretherton et al. 1999) and the same number of independent samples N_{time} (sampling uncertainties). We then calculated the difference of Δdev between all pairs of the ensemble. Since all members are realizations from the same stochastic process, we get an estimate of the *pdf* of Δdev for this process. We repeated this for different parameters of the isotropic diffusion process, leading to different spatial degrees of freedom ($N_{spatial}$ from 5 up to 40). We also repeated this bootstrapping approach for different numbers of independent samples (N_{time} from 120 up to 12,000). Additionally we calculated the uncertainties of datasets that are generated from 20 unorthogonal patterns following a bootstrapping approach.

The pattern we got from a random rotation of EOF-1 to EOF-20 and multiplied them with random times series to create a dataset. In this case we get $N_{spatial}$ between 5 and 9 and repeated again the bootstrapping approach for different numbers of independent samples (from 120 up to 12,000). With both approaches we find a good approximation for the expectation and spread of the *pdf* of Δdev . The expectation value is best described by:

$$\varepsilon(\Delta dev_k) \approx dev_k \sqrt{\frac{2 N_{spatial}}{N_{time}}} \quad (4)$$

where k denotes the k th DEOF mode. Thus the expectation value differs from the North's rule of thumb only by the factor $\sqrt{N_{spatial}}$. It seems reasonable to assume that the expectation of Δdev would depend on the number of independent modes in the domain ($N_{spatial}$), as we have maximized Δdev by pairwise rotation of all leading modes. The standard deviation (*stdv*) of the *pdf* of Δdev follows North's rule of thumb:

$$\text{stdv}(\Delta dev_k) \approx dev_k \sqrt{\frac{2}{N_{time}}} \quad (5)$$

With Eqs. (4) and (5) we can calculate the significance of the DEOF-modes: A DEOF mode that has a Δdev larger than $\varepsilon(\Delta dev) + \text{stdv}(\Delta dev)$ passes the 86 % confidence level and a Δdev larger than $\varepsilon(\Delta dev) + 2 \cdot \text{stdv}(\Delta dev)$ passes the 96 % confidence level. In Fig. 1 two *pdfs* of the Δdev for $N_{spatial} = 10$ (Fig. 1a) and $N_{spatial} = 20$ (Fig. 1b) are shown. Our estimated *pdf* of Δdev (dashed lines) is more conservative than the observed *pdf* (solid lines) and the cumulative distribution curve can be used to estimate the significance of a Δdev value for a given N_{time} .

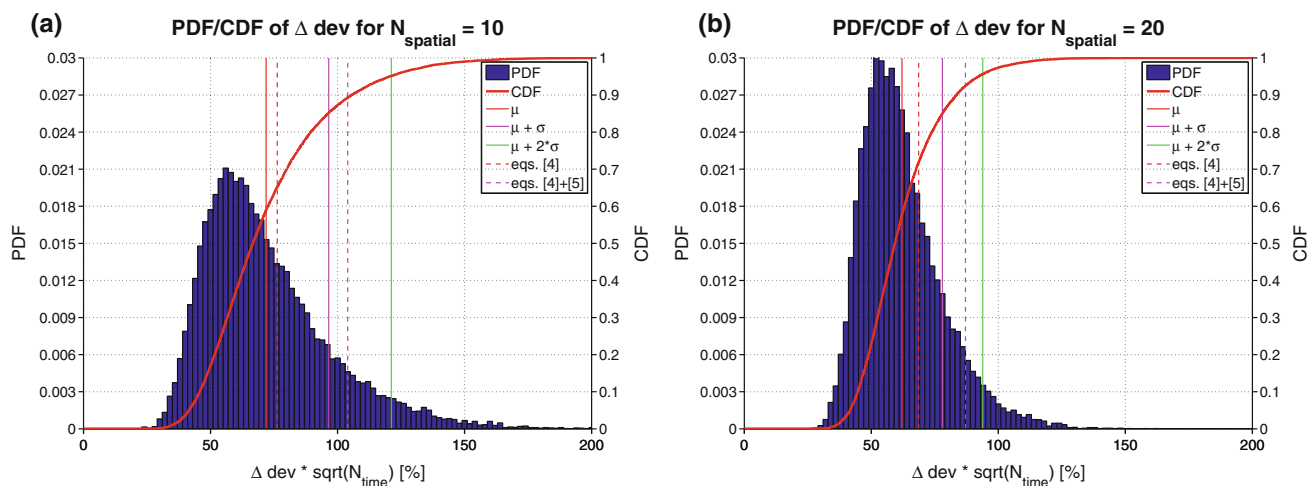


Fig. 1 Probability density function (*pdf*) (blue bars), cumulative distribution function (*cdf*) (red line) of $\Delta dev * \sqrt{N_{time}}$; all values for different numbers of independent samples $N_{times} = 120$ up to 12000 are show in this figure; the *dashed lines* are our estimates of the *pdf*

according Eqs. (4) and (5); in **a** for spatial degrees of freedom $N_{spatial} = 10$ (according to Bretherton et al. 1999) and in **b** for $N_{spatial} = 20$

5 Discussion of some artificial examples

In the following we discuss four artificial examples that increase in complexity, to illustrate how this method detects prescribed changes. The four examples are chosen in a way, that we can see how some simple types of changes are revealed in the DEOF analysis. Although, the changes in climate variability can be more complex, we will see in the subsequent section that the discussion of these simple artificial examples helps us to interpret the results of observed and simulated phenomena. The artificial examples are summarized in Table 3.

For all following artificial examples we choose the stochastic isotropic diffusion process (Eq. 3), as it is a useful null hypothesis for climate variability and has a well-defined structure of multi-poles in the EOF-modes (for details see D07). The EOF-modes of isotropic diffusion depend only on the domain dimensions and the decorrelation length. The latter is here a function of damping coefficient c_{damp} and diffusion coefficient $c_{diffuse}$. The EOF-1 mode is a monopole, the second and third mode are dipoles followed by multi-poles (for details see D07).

The artificial examples we discuss here are all well-defined and the differences between the two artificial datasets are known by construction. In the first two examples we discuss two datasets, which only differ in the strength of the variability of a fixed pattern. In the third example we discuss two datasets in which the position of a dominant mode of variability is different whereas in the last example the multivariate structure of the variability differs in length scale.

5.1 Different fixed teleconnection patterns

In the first example we add a fixed forcing pattern on top of an isotropic diffusion process:

$$\frac{d}{dt}\Phi(\vec{x}, t) = c_{damp} \cdot \Phi(\vec{x}, t) + c_{diffuse} \cdot \nabla^2 \Phi(\vec{x}, t) + f(\vec{x}, t) + \pi(\vec{x}) \cdot F(t) \tag{6}$$

with $\pi(\vec{x})$ as the fixed forcing pattern and $F(t)$ as temporal white noise. The isotropic diffusion processes are calculated on a 77×71 grid point domain, but for EOF analysis only the inner 37×31 grid points are chosen as the data basis to avoid boundary effects. The datasets are driven by different white noise $f(\vec{x}, t)$ and $F(t)$, so that the differences between two datasets are a result of the different forcing patterns and sampling uncertainties. The datasets in this example have 2,400 independent time samples, a decorrelation length of about 9 grid points and $N_{spatial}$ of about 13.

We choose in this first example two different (orthogonal) dipoles as forcing patterns, a left-to-right dipole in dataset \mathcal{A} and a top-to-bottom dipole in dataset \mathcal{B} (Fig. 2a, b). The shape and strength of these two forcing patterns

were chosen in a way that they would result as the EOF-2 modes in each dataset. Note, that in a continuous stochastic process such as isotropic diffusion (Eq. 3) all possible patterns of variability exist (explain a non-zero amount of variance). The left-to-right dipole pattern would explain 10.0 % in \mathcal{A} and the top-to-bottom dipole 8.3 % in \mathcal{B} in the pure isotropic diffusion process (the background noise). By including the forcing pattern in \mathcal{A} we increase the amount of variance explained of this pattern in dataset \mathcal{A} by 6.0 % and by including the forcing pattern in \mathcal{B} we increase the amount variance explained of this pattern in dataset \mathcal{B} by 4.2 %. Due to the different forcing patterns the variability is higher in the left and right part of the domain in \mathcal{A} and in the top and bottom part in \mathcal{B} (Fig. 2c).

We start the discussion of the differences of the spatial structure in the variability of the two datasets by comparing the leading EOF-modes (see Fig. 3a–f). The three leading EOF-modes of the two datasets are similar in pattern and explained variances, but the order of the patterns are different for mode 2 and 3. This reflects the fact that the left-to-right dipole pattern explains more variance in dataset \mathcal{A} and the top-to-bottom dipole pattern explains more variance in dataset \mathcal{B} , as we forced it by construction. These differences are quantified in the eigenvalue spectra (see Fig. 3g, j). It is first of all important to note, that the x-axes in Fig. 3g and j refer to different sets of EOF-modes in general and the eigenvalues can therefore not be compared against each other directly. The left-to-right dipole pattern of dataset \mathcal{A} , for instance, is the mode number two in Fig. 3g, which is similar, but not identical to mode number three in Fig. 3j. So in order to be able to compare the relative importance of a specific pattern in both datasets we have to compare the $ev_i^{\mathcal{A}}$ values against the values $pev_i^{\mathcal{A} \rightarrow \mathcal{B}}$ or the $ev_i^{\mathcal{B}}$ values against the values $pev_i^{\mathcal{B} \rightarrow \mathcal{A}}$. In Fig. 3g, j we see that projected explained variances ($pev_i^{\mathcal{A} \rightarrow \mathcal{B}}$ and $pev_i^{\mathcal{B} \rightarrow \mathcal{A}}$) do not have to be monotonically decreasing as explained variances of EOF analysis. From the projected explained variances we can further see, that the left-to-right dipole has in dataset \mathcal{B} a much lower explained variance and the top–bottom dipole has a larger explained variance, thus showing the change in the hierarchy between EOF-2 and EOF-3, as forced by the construction of the example.

In the next step we can now find the leading DEOF patterns that maximize the differences between the two datasets by pairwise rotations of the EOF-modes. DEOF-1 ^{$\mathcal{A} \rightarrow \mathcal{B}$} (Fig. 3h) is a left-to-right dipole with an explained variance of 16.0 % in \mathcal{A} and 9.3 % in \mathcal{B} , thus a difference of 6.7 %, statistical significant according the test in Sect. 4. This pattern is very similar to the EOF-2 in \mathcal{A} , EOF-3 in \mathcal{B} and the forcing pattern in \mathcal{A} . The DEOF-2 ^{$\mathcal{A} \rightarrow \mathcal{B}$} (Fig. 3i) has no significant spatial structure and reflects the different white noise forcing (see further below for a discussion of

Table 3 Summary of all examples

Example name	Type of differences	DEOF characteristics
5.1 Different fixed teleconnection patterns	One leading mode in each data set is different from the other data set	One or more eigenvalues will be more dominant in both datasets relative to the other dataset One (only one!) DEOF-mode will be significantly dominant in each of the two datasets
5.2 Intensification of a fixed pattern	One leading in one data set mode is stronger than in the other	One or more eigenvalues will be more dominant in one dataset relative to the other dataset One (only one!) DEOF-mode will be significantly dominant in the one dataset relative to the other dataset
5.3 Shift of the location of a fixed pattern	One leading mode has different spatial location in the two datasets	One or more eigenvalues will be more dominant in both datasets relative to the other dataset One (only one!) DEOF-mode will be significantly dominant in each of the two datasets The DEOF-modes peak at the locations where the variance is increased most relative to the other dataset, marking the location shift
5.4 A Multivariate difference: A difference in length-scale	The length scale of the multivariate stochastic process is different in the two data sets	Most leading eigenvalues will be more dominant in one dataset relative to the other dataset The higher-ranked eigenvalues of the other data set maybe more dominating than in the first dataset Two or more DEOF-modes will be significantly dominant in the first dataset relative to the other dataset More than one large-scale leading EOF-mode will be more dominant than in the other dataset
6.1 Sea Level Pressure over the North Atlantic and Europe in winter	Mainly a pattern shift in the EOF-1 as in 5.3 and S4	One eigenvalue dominates in both datasets relative to the other dataset One DEOF-mode significantly dominates in each of the two datasets The DEOF-modes peak at the locations where the variance is increased the most relative to the other dataset, marking the location shift
6.2 Sea Level Pressure of the Southern Hemisphere in DJF	Mainly a pattern shift in the EOF-1 as in 5.3 and S6	One eigenvalue dominate in both datasets relative to the other dataset One DEOF-mode significantly dominates in each of the two datasets The DEOF-modes peak at the locations where the variance is increased the most relative to the other dataset, marking the location shift
6.3 Northern Hemispheric winter surface temperature	Mainly a pattern shift in the EOF-1 as in 5.3 and S4, but also some difference in the patterns as in 5.1	Several eigenvalues dominate in both datasets relative to the other dataset One DEOF-mode significantly dominates in each of the two datasets The DEOF-modes peak at the locations where the variance is increased the most relative to the other dataset, marking the location shift
6.4 North Pacific SST	Mainly an intensification in parts of EOF-1 (or the variance in this region) as in 5.2, but also some similarity to a shift as in 5.3	Two eigenvalues dominate in the 21C dataset relative to the 20C dataset One DEOF-mode significantly dominates in each of the two datasets The DEOF-modes peak at the locations where the variance is increased most relative to the other dataset. With the 21C DEOF-mode being more dominant
6.5 Precipitation over the tropical Indo-Pacific	Mainly a multivariate change in the modes of variability as in 5.4, with some characteristics of a shift in the EOF-1 as in 5.3	Several eigenvalues dominate in the 20C dataset relative to the 21C dataset and one eigenvalue of 21C dominates over the 20C dataset Two DEOF-modes significantly dominate in each of the two datasets

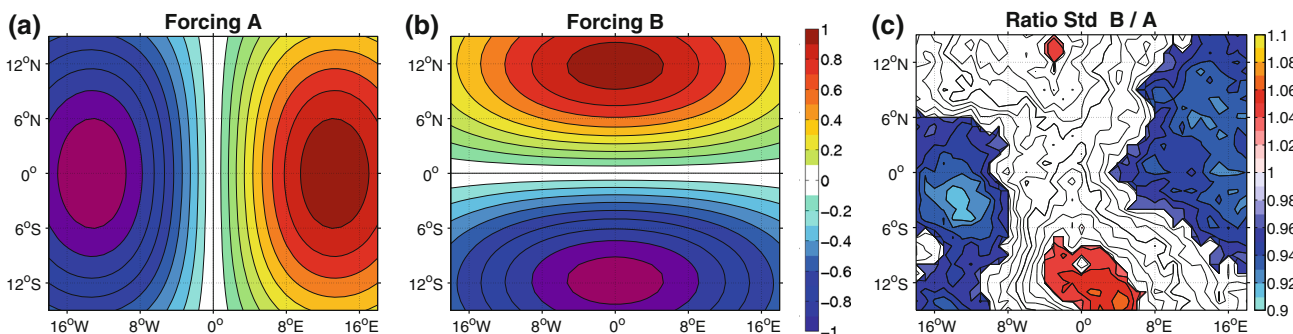


Fig. 2 **a** The forcing pattern, that was used in the first dataset \mathcal{A} , in **b** in the second dataset \mathcal{B} (colorbar in arbitrary units) and in **c** the ratio of the standard deviation of the second dataset divided by the

first dataset is given, with shading indicating statistical significant changes according to a Fisher-F test with 90 % confidence level

significance and uncertainties). This indicates that the dataset \mathcal{A} has one and only one pattern of variability (DEOF-1 $^{\mathcal{A} \rightarrow \mathcal{B}}$ in Fig. 3h) that is more dominant in dataset \mathcal{A} than in dataset \mathcal{B} . In turn for dataset \mathcal{B} we find the top-to-bottom pattern as the significant DEOF-1 $^{\mathcal{B} \rightarrow \mathcal{A}}$ (Fig. 3k). The DEOF-2 $^{\mathcal{B} \rightarrow \mathcal{A}}$ (Fig. 3l) is not significant and is therefore again indicating that the top–bottom dipole is the only pattern that is more dominant in dataset \mathcal{B} than in dataset \mathcal{A} , as expected by construction of this example.

The significance of Δdev was calculated using the Eqs. (4) and (5) with an 86 % confidence level. Alternatively we can estimate it from Fig. 1a, b: with a $\Delta dev = 6.7\%$ and $N_{times} = 2,400$ we get $\Delta dev \cdot \sqrt{N_{times}} = 328$. With $N_{spatial} = 13$ we find that this value is roughly at the 100 % value (none of the numerical realizations produced such a large Δdev).

According to the significance test both DEOF-1 patterns have a significant Δdev , while the higher ordered DEOF patterns are all insignificant. Thus our test can separate the signal from the noise. The strength of the forcing patterns in this example was constructed in a way, that we would expect a difference of 6.0 % in DEOF-1 $^{\mathcal{A} \rightarrow \mathcal{B}}$ and of 4.2 % in DEOF-1 $^{\mathcal{B} \rightarrow \mathcal{A}}$, as mentioned above. The estimated values in this example (Fig. 3h, k) match the expected values relatively well.

In summary, we have illustrated in this example that the two different forcing patterns can be identified with this approach quite clearly in a qualitative and quantitative way, even though the forcing patterns are not the dominant modes and even though they project strongly onto the background noise of isotropic diffusion. Additionally, the approach demonstrates that there are no other significant large-scale differences between the two datasets.

5.2 Intensification of a fixed pattern

In the second example we included a forcing pattern in the second dataset only to illustrate how the intensification of a mode is represented in the DEOF analysis. The forcing pattern (Fig. 4a) is a monopole located in the eastern part

of the domain, which increases the variance in this region (Fig. 4b). The shape of the pattern was chosen to be projecting onto both EOF-1 and EOF-2 of the isotropic diffusion process (domain-wide monopole and a left-to-right dipole) to illustrate how a forcing pattern can be detected that does not project on one EOF-mode only.

The EOF-modes (Fig. 5a–d) of the two datasets are quite similar, but the comparison of the eigenvalue spectra reveals some differences. The DEOF-1 $^{\mathcal{B} \rightarrow \mathcal{A}}$ (Fig. 5h) is the only significant DEOF pattern and no other significant DEOF patterns exist in dataset \mathcal{A} . Thus the DEOF analysis is able to reveal the forcing pattern even though its original structure is not projecting on one particular EOF-mode and it shows that only one pattern is amplified in dataset \mathcal{B} . The increase in variance in DEOF-1 $^{\mathcal{A} \rightarrow \mathcal{B}}$ (Fig. 5f) is not significant and reflects the different white noise forcing.

The experiment can also be repeated with more than one fixed forcing pattern included in Eq. (6) for dataset \mathcal{B} , to test if the intensification of several modes can be detected. The method can clearly present several fixed forcing patterns, assuming that they are orthogonal to each other (see Supplemental Figure S1 and S2).

5.3 Shift of the location of a fixed pattern

In the third example we introduce a forcing pattern that shifts the location between dataset \mathcal{A} and dataset \mathcal{B} (Fig. 6a, b), so that the forcing weakens in one part and strengthens in the other (Fig. 6c) and describes an eastward shift of the forcing by 16 grid points. The two EOF-1 modes are slightly different in shape, with the center more to the left in dataset \mathcal{A} and more on the right in \mathcal{B} (Fig. 7a–d), consistent with the forcing patterns. The eigenvalue spectra reveal differences between the two datasets in EOF-1 and EOF-2 (Fig. 7e) and the DEOF-1 of both projections reveal larger and significant differences. Thus in this example, the DEOF-1 patterns of both projections reveal a dominant pattern in each dataset, together illustrating the shift in a pattern.

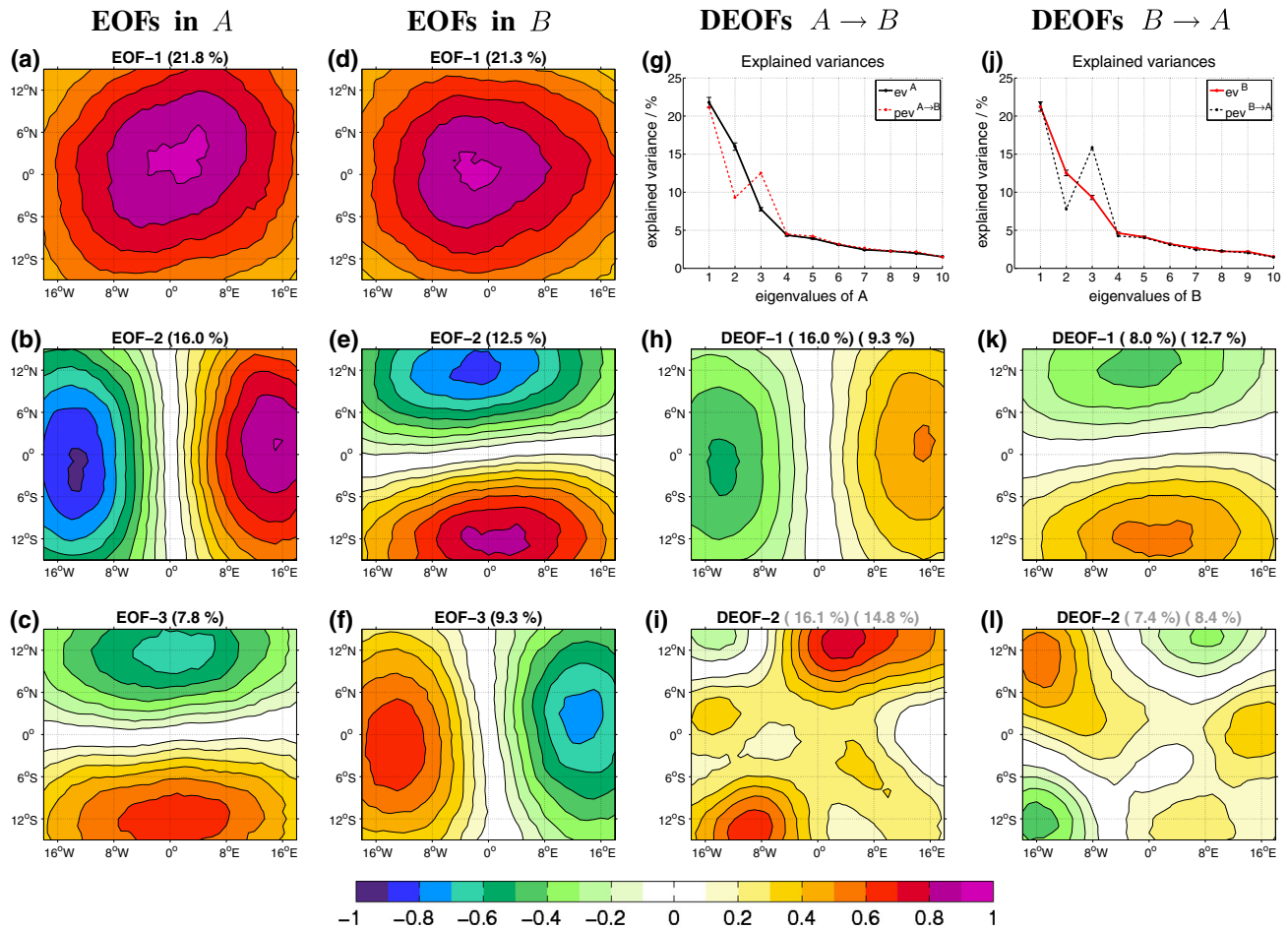
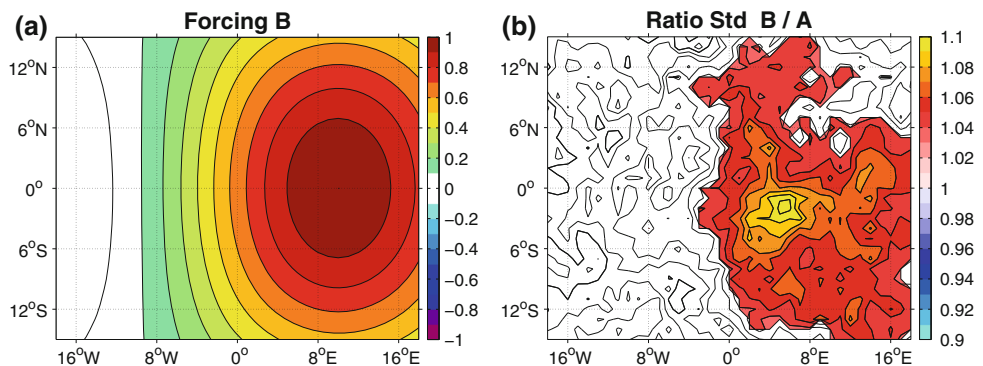


Fig. 3 a–c EOF patterns of dataset A (colorbar in arbitrary units); d–f EOF patterns of dataset B ; explained variance is given in the header in brackets; g the explained variances of the eigenvalues of the dataset A (black) and explained variances of dataset A projected onto the eigenvalues of dataset B (red dashed), the error bars show the statistical uncertainties of the eigenvalues due to sampling errors according to North et al. (1982); h–i DEOF $^{A \rightarrow B}$ patterns; the

explained variances $dev^{A \rightarrow B}(A)$ and $dev^{A \rightarrow B}(B)$ are given in the header in brackets, respectively, and grey values indicate that Δdev is not significant according the test in Sect. 4; j same as g, but here showing the eigenvalues of dataset B (red) and the explained variances of dataset B projected onto the eigenvalues of dataset A (black dashed), k–l same as h–i, but for the DEOF $^{B \rightarrow A}$ patterns

Fig. 4 Same as Fig. 2, but here for the example in Sect. 5.2



However, we have to note that the pattern shape of the DEOF-1 patterns do not quite match the forcing patterns. This can be understood when we think about how this method works: A DEOF pattern with the shape of the forcing pattern would not maximize in this case the

difference in explained variance between the two datasets, because it also has amplitude at those locations, where the other dataset has more explained variance due to the other forcing pattern. So the interpretation in this case becomes more complicated. Indeed if we compare the first example

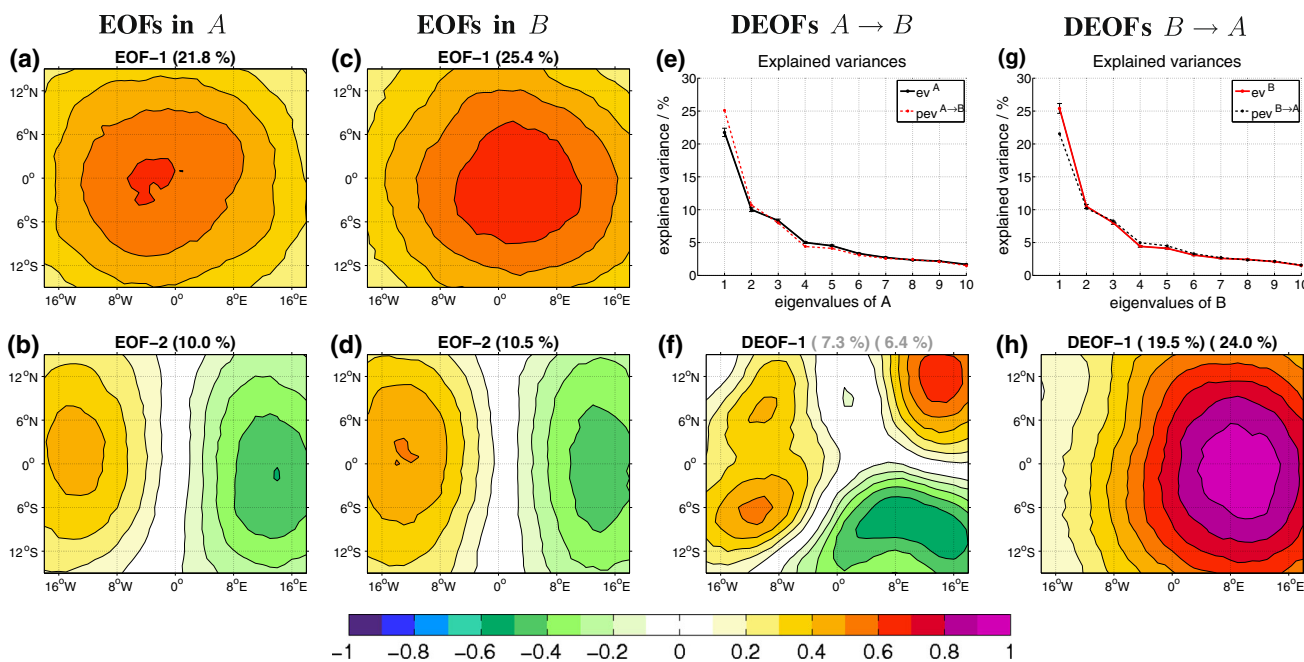


Fig. 5 Same as Fig. 3, but here for the example in Sect. 5.2

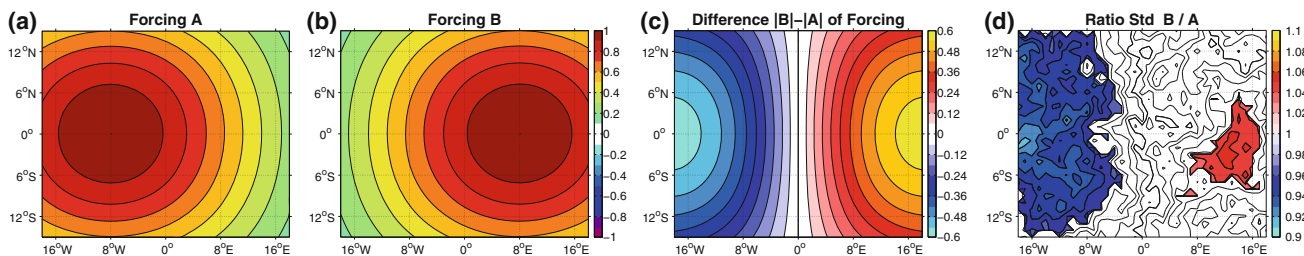


Fig. 6 Same as Fig. 2, but here for the example in Sect. 5.3; additional in c the difference between the two forcings $B - A$

with two different (orthogonal) forcing patterns with this example here, we can notice that the two patterns (before and after the shift) here are not orthogonal to each other (they project onto each other). In principle the first example can also be interpreted as a shift in one pattern: The forcing pattern in dataset A is the forcing pattern in dataset B rotated by 90° . The shift in this first example is more complete, leading to two (before and after the shift) orthogonal patterns.

So the signature of a shift of one pattern is that we have a significant DEOF-1 mode in both projections, each representing a pattern that is similar to the pattern that is shifted. The fact that the patterns before and after the shift are not orthogonal to each other will lead to the DEOFs being slightly different from the pattern that is shifted. Thus we get two patterns, each of them mostly similar to one “sign” of the ratio of standard deviation (Fig. 6d). Other examples with a shifted dipole pattern are shown in the Supplemental Figures S3 to S6.

5.4 A multivariate difference: a difference in length-scale

In this last artificial example we compare two pure isotropic diffusion processes with different length-scales. So no fixed forcing patterns are included. This example can illustrate that differences in the EOF-modes do not always have to be interpreted as a difference in a fixed pattern, but may sometimes reflect multivariate differences in the stochastic high-dimensional process underlying the dataset. In comparison with the above examples the discussion of this example illustrates the characteristic signatures of multivariate (high-dimensional) differences.

In dataset A we choose a weaker damping and diffusion constants than in dataset B , which leads to a shorter decorrelation length (about 7 grid points) in dataset A and a larger decorrelation length (about 10 grid points) in dataset B . The pattern shape of the EOF-modes is similar in both datasets (Fig. 8a–f), which we also see in the eigenvalues,

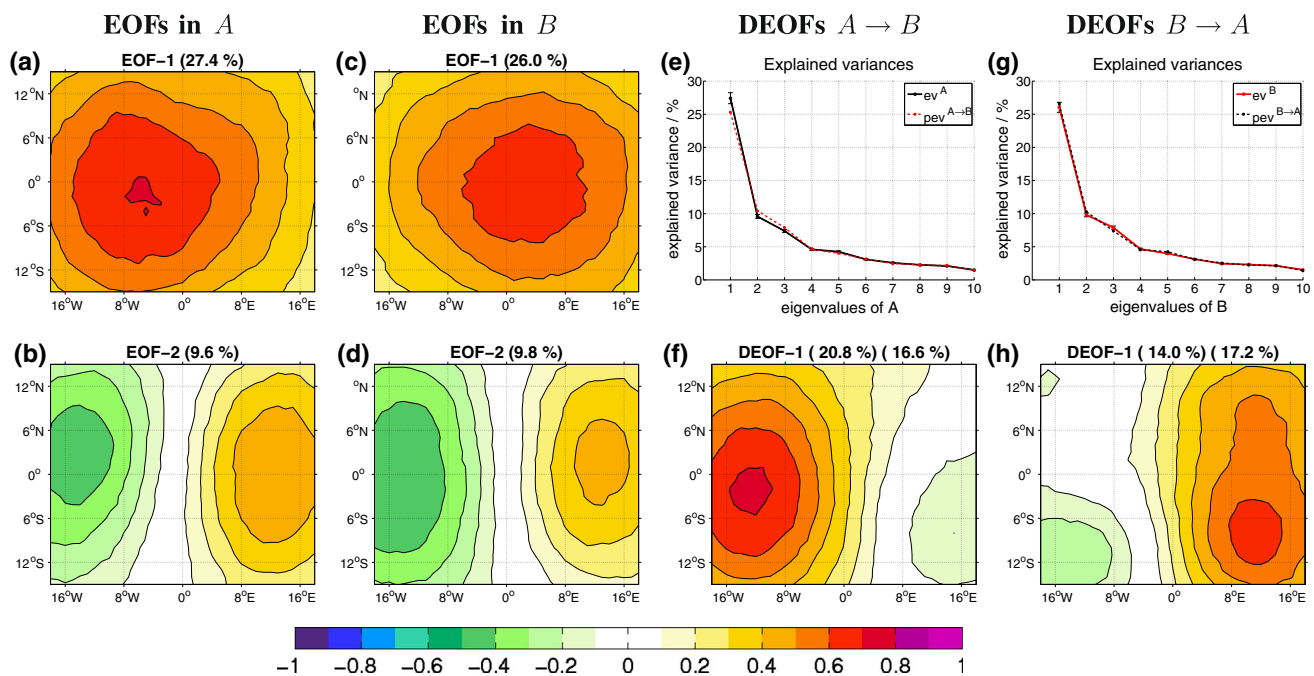


Fig. 7 Same as Fig. 3, but here for the example in Sect. 5.3

as the black dashed line of Fig. 8j is nearly the same as the black solid line in Fig. 8g (same for the two red lines). But the amount of explained variance is different. The shorter decorrelation length in dataset \mathcal{A} leads to larger number of spatial degrees of freedom compared to dataset \mathcal{B} and subsequently more EOF-modes are needed to explain the same amount of variance. Therefore the leading EOF-modes have to explain less variance and the higher order EOF-modes have to explain more variance to sum up to 100 %.

The first three leading $\text{DEOF}^{\mathcal{B} \rightarrow \mathcal{A}}$ are similar to the first three EOF patterns and are all significantly stronger in dataset \mathcal{B} than in dataset \mathcal{A} . This is quite different from the previous examples, where we always found only one pattern that was more dominant in one of the datasets. It thus suggests that the differences in the two datasets are of a higher-dimensional order and are most likely not best described by the change in one, two or three patterns but are more likely a reflection of a change in the stochastic high-dimensional process underlying the dataset, such as a change in decorrelation length. In turn the $\text{DEOF}^{\mathcal{A} \rightarrow \mathcal{B}}$ are all of small-scale structure and reflect the relative increase in variance of small-scale variability, with first two $\text{DEOF}^{\mathcal{A} \rightarrow \mathcal{B}}$ being significant (Fig. 8h–i).

5.5 Summary

We illustrated the application of the DEOF analysis with a series of well-defined examples. By analyzing the spectrum

of eigenvalues in comparison with the projected explained variances we can see how distinct the EOF patterns are and with the DEOF patterns we are able to specify the pattern that most strongly gains or loses importance and to quantify how much explained variance is gained or lost.

The discussion of the idealized examples is summarized in Table 3. The table can be used as look up table to identify the structures that describe the difference in real data analysis problems. If a single mode or teleconnection is amplified in dataset \mathcal{B} compared to a dataset \mathcal{A} it appears as the $\text{DEOF-1}^{\mathcal{B} \rightarrow \mathcal{A}}$, but no significant $\text{DEOF}^{\mathcal{A} \rightarrow \mathcal{B}}$ will appear (second example in Table 3). If a pattern shifts its position in dataset \mathcal{B} compared to its position in dataset \mathcal{A} , then both the leading $\text{DEOF}^{\mathcal{A} \rightarrow \mathcal{B}}$ and the $\text{DEOF}^{\mathcal{B} \rightarrow \mathcal{A}}$ pattern together highlight the shift (third example in Table 3). And last a change in the multivariate structure is reflected in having several significant DEOF patterns in either one projection or in both, depending on the nature of the multivariate changes (fourth example in Table 3).

6 Literature examples about climate change simulations

In this section we discuss examples from the literature to illustrate how this method relates to other approaches. In all cases we discuss previous studies that analyzed the changes in the spatial structure of climate variability from 20th century control climate to future 21th century global

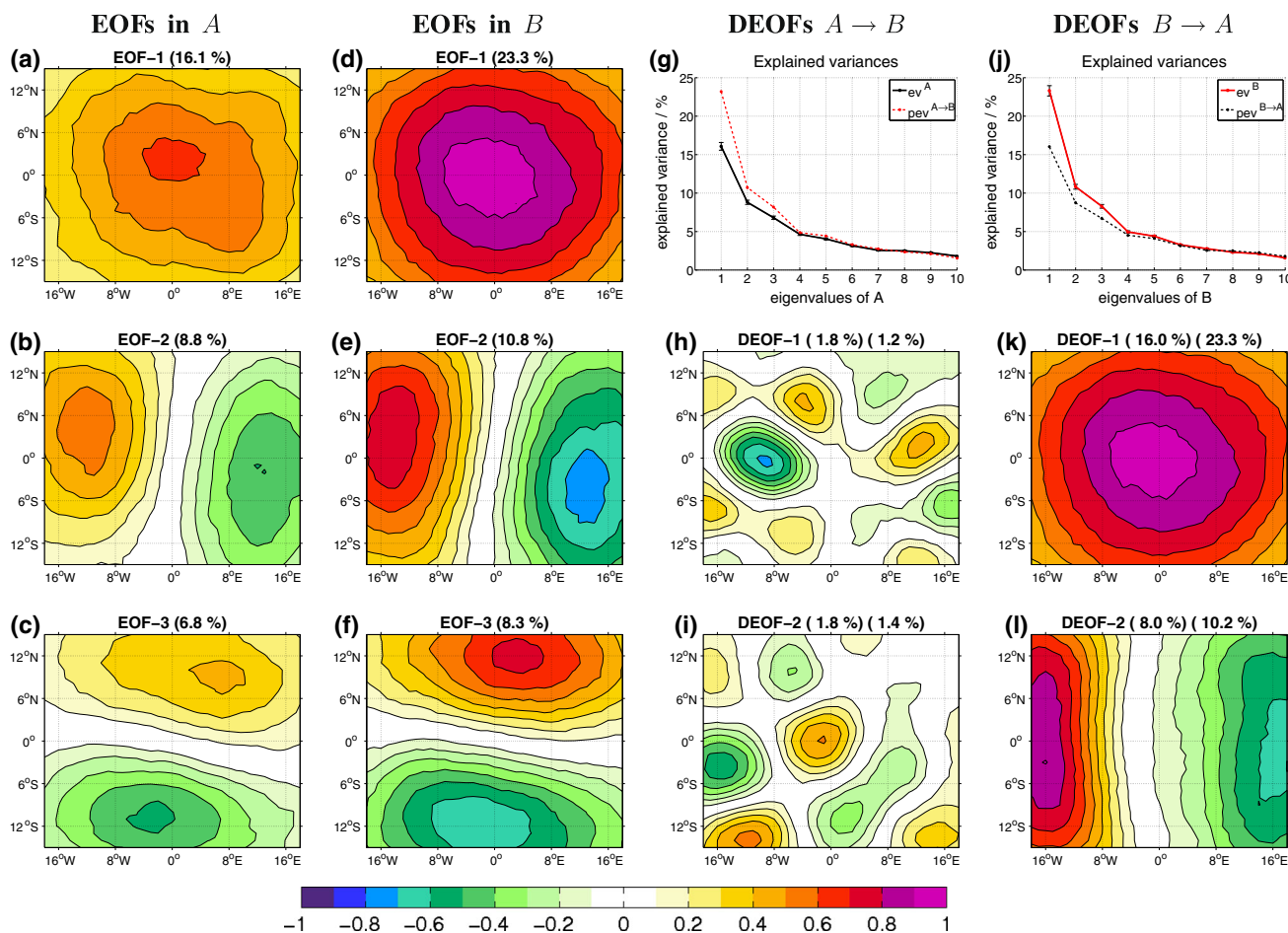


Fig. 8 same as Fig. 3, but here for the example in Sect. 5.4

warming scenarios with different methods. Some of these methods are based on EOF-modes and others are based on alternative methods. In all examples the discussion is about the change of modes under climate change. Thus to test our method we try to reproduce with our method the results of several previous studies in a multi model ensemble from the CMIP3 data base. In the following examples the dataset \mathcal{A} refers to the period 1950–1979 in the present day or 20th century control climate (dataset 20C) and dataset \mathcal{B} to the period 2070–2099 future 21th century or global warming scenario climate (dataset 21C). The focus in the discussions will be on illustrating the robustness of the method introduced in this study and not on arguments about changes in the modes of variability in the future, although the discussion may contribute to the latter.

6.1 Sea level pressure over the North Atlantic and Europe in winter

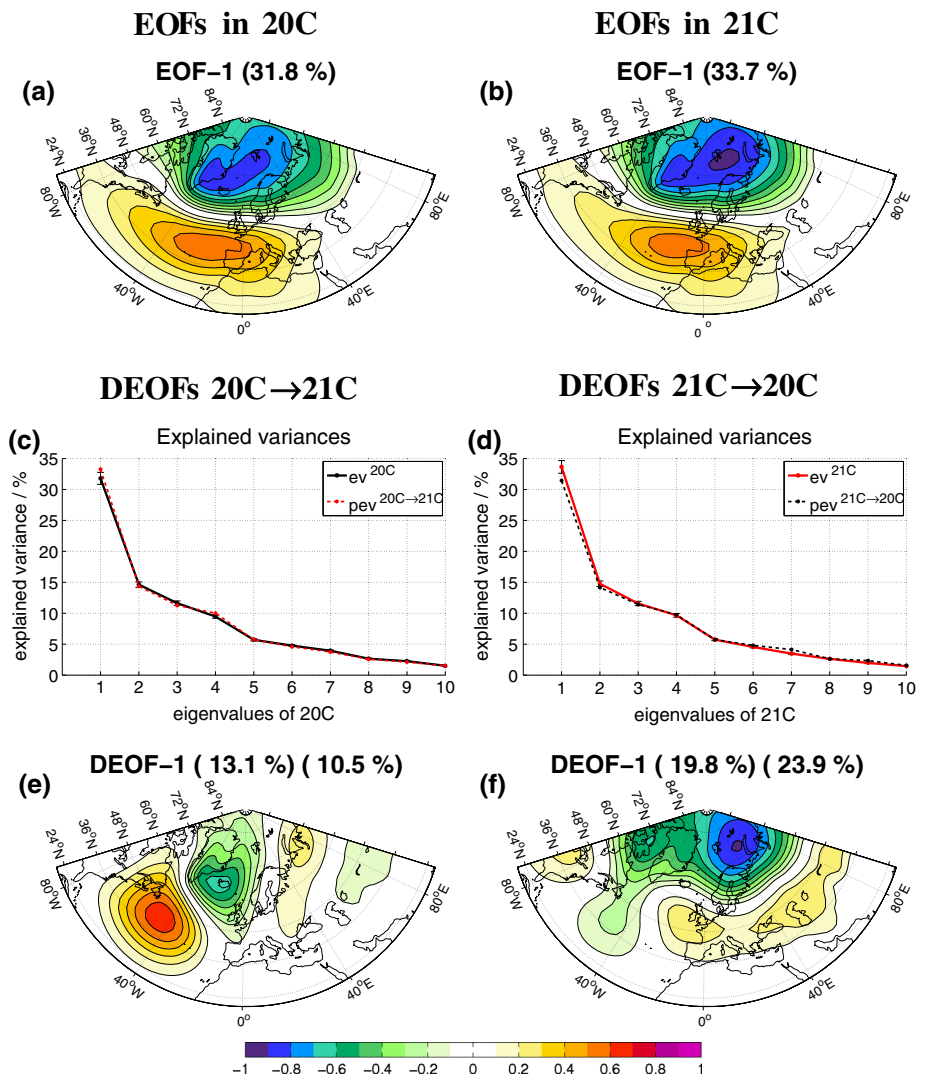
Hu and Wu (2004) investigated the two centers of action of the North Atlantic Oscillation (NAO) in winter SLP of the coupled ECHAM4/OPYC3 climate model, which they

defined by the strongest negative correlation between two grid points in this region, and found a northeastward shift of both centers of the NAO in global warming.

The EOF analysis in winter SLP of the CMIP3 multi model ensemble shows in both periods as EOF-1 the typical NAO pattern (Fig. 9a, b), with only small differences: The negative pole gets stronger over the Barents Sea in 21C, both centers move a little bit to the east and the explained variance is 2.1 % higher in 21C as in 20C. These changes appear to be small by visual inspection or pattern correlation (0.99).

The DEOF-1^{20C→21C} (Fig. 9e) shows a significant decrease in explained variance of 2.6 % in 21C in a dipole structure over the western Atlantic. The DEOF-1^{21C→20C} (Fig. 9f) shows a significant increase in explained variance of 4.3 % in a dipole structure over the polar region and the midlatitudes of the east Atlantic and Eurasia. This structure with significant DEOF-1 in both projections is similar to the artificial examples with the pattern shift (Sect. 5.3 or Supplemental Fig. S3 and S4): Losing relevance over the western Atlantic in 20C and gaining relevance over the Polar Regions, the eastern Atlantic and Eurasia in 21C.

Fig. 9 same as Fig. 3, but here for DJF SLP over the Atlantic region in the periods 1950–1979 (20C) compared with the period 2070–2099 (21C), as discussed in Sect. 6.1



These DEOF-1 patterns together mark the northeastward shift of the NAO pattern in global warming, as already mentioned in Hu and Wu (2004) and fit quite well to the

change in variability in Fig. 10. Additionally we can see, that the NAO pattern strengthens strongest over the Barents sea, a region that could be important for the Northern Hemisphere in global warming, as also mentioned in Petoukhov and Semenov (2010). In summary, the DEOF analysis basically confirms the Hu and Wu (2004) results, illustrating the robustness of the method in this context.

Ratio Std DJF SLP 21C / 20C

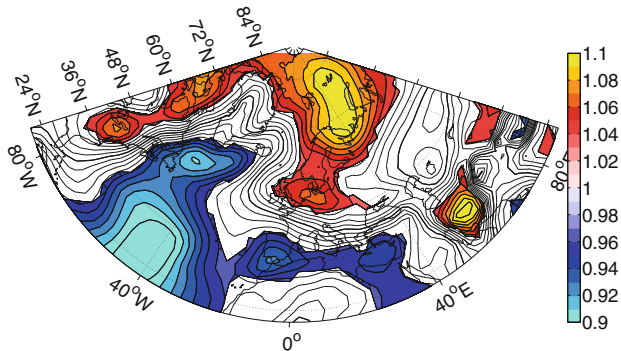


Fig. 10 Ratio of the standard deviation of 21C divided by 20C for DJF SLP over the Atlantic region, with shading indicating statistical significant changes according a Fisher-F test with 90 % confidence level

6.2 Sea level pressure of the Southern Hemisphere in DJF

Kidston and Gerber (2010) analysed the position of the Southern Hemispheric eddy-driven jet stream by looking at the maximum in zonal mean near surface zonal wind speed in the CMIP3 data base and found a pole-ward shift of the jet under global warming, which also leads to a pole-ward shift of the Southern Annular Mode (SAM).

In the EOF analysis of DJF SLP in the Southern Hemispheric higher latitudes the EOF-1 pattern (SAM),

Fig. 11 Same as Fig. 9, but here for Southern Hemispheric SLP in DJF as discussed in Sect. 6.2

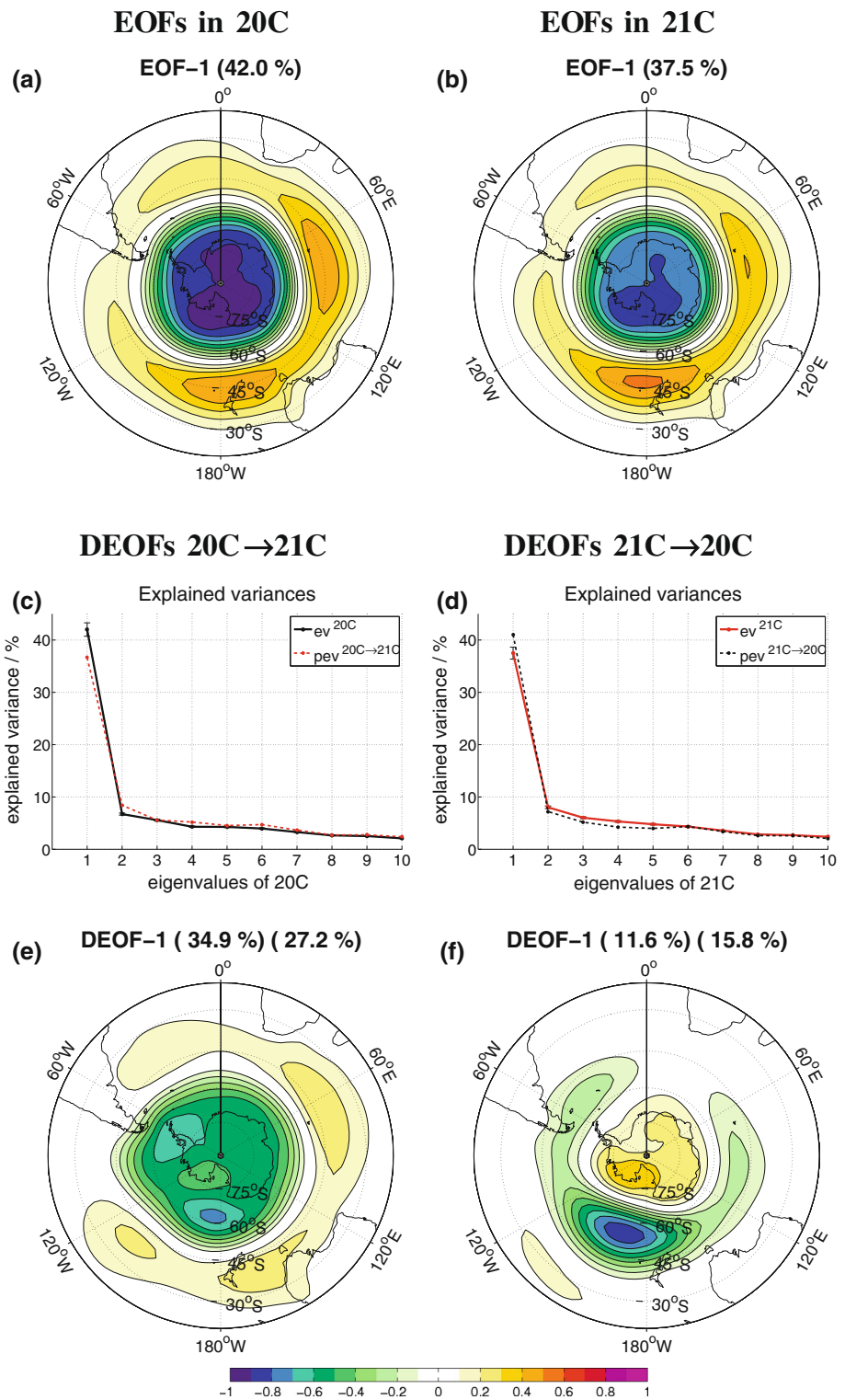


Fig. 11a, b) is by far the most dominant but loses 4.5 % of its explained variance in 21C in comparison to 20C. The annular pattern shifts pole-ward in 21C and the amplitude weakens a little bit. Again these changes can hardly be seen by visual inspection or by pattern correlation (0.99). The

DEOF-1^{20C→21C} (Fig. 11e) shows an almost annular pattern that has a 7.7 % higher explained variance in 20C than in 21C. This pattern is located further equator-ward than the EOF-1 pattern. The DEOF-1^{21C→20C} (Fig. 11f) is also almost annular but with a maximum over the Pacific and

has a 4.2 % higher explained variance in 21C than in 20C. This structure is more pole-ward than the EOF-1 pattern. In comparison with the artificial example in Sect. 5.3 and Supplemental Fig. S5 and S6 it becomes clear, that these two DEOF pattern together reveal the pole-ward shift of the SAM pattern, consistent with the study of Kidston and Gerber (2010). Again it illustrates the robustness of the DEOF analysis. Additionally, it could be noted here, that this shift is most pronounced over the South Pacific.

6.3 Northern hemispheric winter surface temperature

The third example is the winter T_{surf} of the Northern Hemisphere. In Keeley et al. (2008) T_{surf} was investigated in a $2 \times \text{CO}_2$ and $4 \times \text{CO}_2$ slab ocean run in comparison to a control run. EOF analysis was performed to find the patterns of variability and pattern correlations between individual EOF-modes to find the differences in the modes between the control and increased CO_2 runs. They found no significant changes in terms of dominance or spatial pattern in the modes of variability.

The leading EOF-modes in the CMIP3 multi model ensemble in both the control 20C simulations and the 21C scenario simulations (which corresponds roughly to the analysis of Keeley et al. 2008) are shown in Fig. 12. The EOF-1 modes in both centuries are mostly the manifestation of the NAO in T_{surf} (Hurrell and Van Loon 1997). The leading EOF-modes in the multi model ensemble simulations are indeed very similar. Not only are the patterns quite similar (pattern correlation = 0.94), but also are the explained variances not too different. However, the eigenvalue spectra of the 20C and 21C multi-model ensemble dataset relative to the projected eigenvalues $pev_i^{20C \rightarrow 21C}$, and $pev_i^{21C \rightarrow 20C}$ reveal some quite significant difference, also in the spatial structure.

The DEOF-1^{20C→21C} (Fig. 12e) is a multi-pole structure, with strongest amplitude over the Barents Sea, the Labrador Sea and Alaska. This pattern shows a significant decrease of explained variance of 2.9 % (a reduction of one-third relative to its eigenvalue) from 20C to 21C. The DEOF-1^{21C→20C} (Fig. 12f) projects strongly on the EOF-1 pattern, but is shifted more to the east over Eurasia. This pattern shows a significant increase in explained variance of 2.8 % from 20C to 21C, which represents a 30 % increase relative to the explained variance of this mode in the 20C control simulation. Both DEOF-1 modes together reveal an eastward shift of the NAO manifestation in T_{surf} in 21C, with an increase in dominance over Asia and a decrease over the Barents Sea and Scandinavia. This eastward shift could be expected from shift of NAO in winter SLP in Sect. 6.1. But also the changed snow and sea ice conditions seem to have an effect on T_{surf} , by reducing

the amount of variability over Alaska and the Labrador Sea in 21C.

Thus in contrast to the study of Keeley et al. (2008) our method reveals significant changes in the spatial pattern of the modes variability. This may, to some degree, be due to the larger database used here (24 CMIP3 models) and using transient global warming simulations, in contrast to Keeley et al. (2008) who used only one $2 \times \text{CO}_2$ and $4 \times \text{CO}_2$ global warming simulation of one climate model. But it also illustrates the robustness of the method presented here.

6.4 North Pacific sea surface temperature

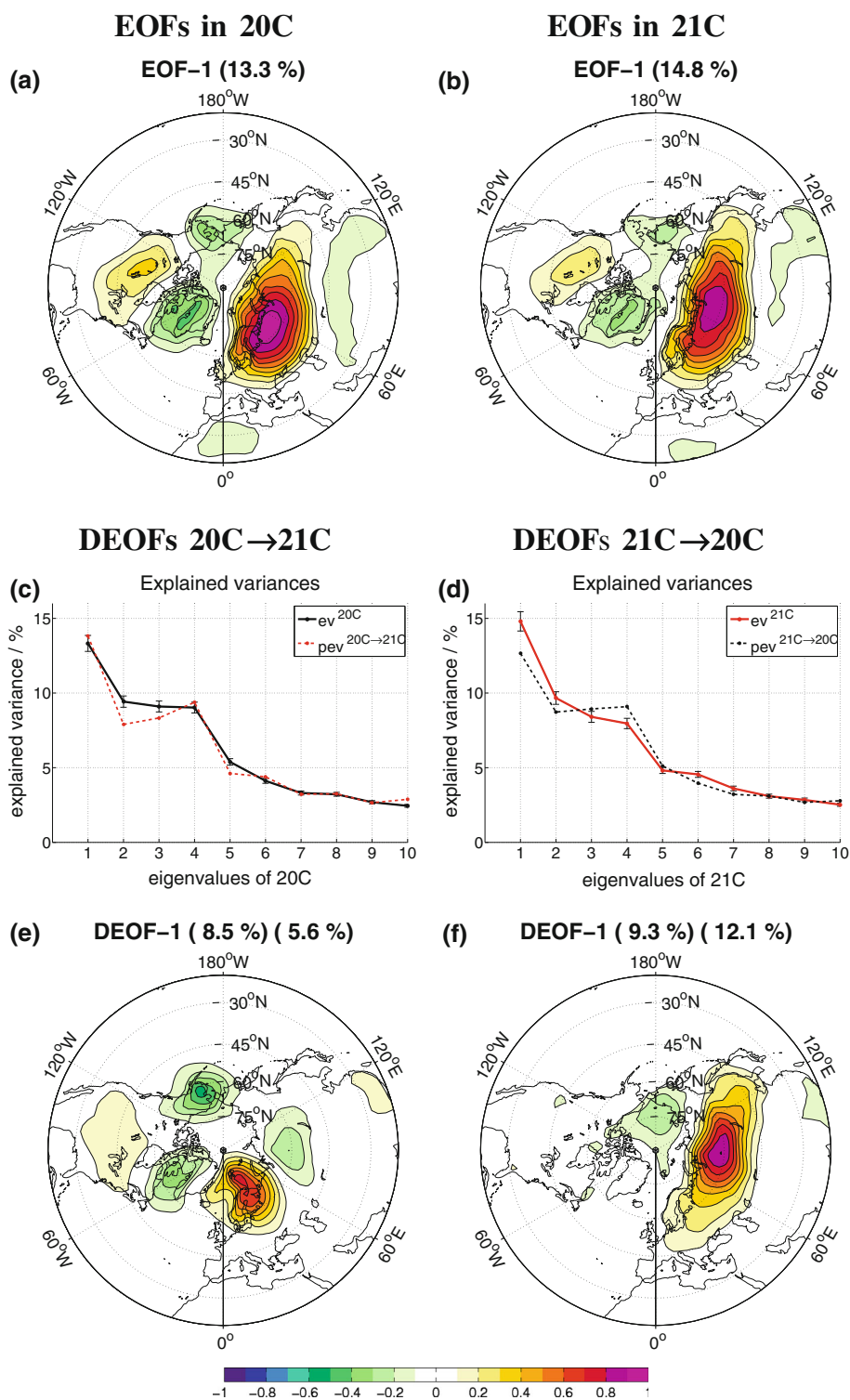
The next example is SST of the North Pacific for the periods 1950–1999 (20C) and 2050–2099 (21C). We choose here 50 years long periods, because the Ocean has a longer decorrelation time, thus fewer independent samples. The Pacific Decadal Oscillation (PDO) is the dominant mode of variability of North Pacific SST and in Furtado et al. (2011) its change in global warming was investigated in the same multi model ensemble of 24 IPCC models from the CMIP3 database. They did not mention which method they used to compare the two EOF sets, but found no significant changes in the patterns of variability.

In both centuries the EOF-1 (Fig. 13a, b) represents the PDO and again the modes are quite similar in pattern (pattern correlation = 0.98) and explained variances. However, the DEOF-1^{21C→20C} (Fig. 13f) finds a significant increase in variance in a pattern centered in the subtropical southeast corner of the domain. This modes variance is increasing by roughly one-third relative to its variance in the 20C simulations. The overall change in modes is somewhat similar to the artificial example 2 with the intensification of a pattern. The strong variability increase over the subtropical region further supports this view (not shown). However, the change in modes in the North Pacific also has some aspects of a shift in a pattern. This is supported by fact that the DEOF-1^{21C→20C} and DEOF-1^{20C→21C} both project onto the EOF-1, but both representing different aspects or locations of the EOF-1 mode. Thus it could be interpreted as a shift in the teleconnection of this mode from the extra-tropics more to the eastern subtropics of the North Pacific.

6.5 Precipitation over the tropical Indo-Pacific

Hu et al. (2012) analysed the global warming response of tropical precipitation in the CCSM3 climate model in all four seasons and compared EOF-modes of the control scenario with the EOF-modes of the A1B scenario. They found some small differences in the details, but overall a high pattern correlation of the leading EOF-modes let them

Fig. 12 Same as Fig. 9, but here for Northern Hemispheric T_{surf} in DJF as discussed in Sect. 6.3



conclude that there are no significant differences. Here we will focus our analysis on the Indo-Pacific region as the leading modes of variability of tropical precipitation are all located in this region (see Figs. 11 and 12 of Hu et al. 2012), but the results would be the same, if we would take the whole tropics.

The variability of precipitation has a small decorrelation length, thus has a lot of small scale variability (Fig. 14a–f). The projected eigenvalues show that the pattern shape has changed. The DEOF-1^{21C→20C} (Fig. 14k) is a multi-pole structure quite different from the EOF-1 pattern that has a significant increase in variance. The variance in this mode

Fig. 13 Same as Fig. 9, but here for North Pacific SST as discussed in Sect. 6.4

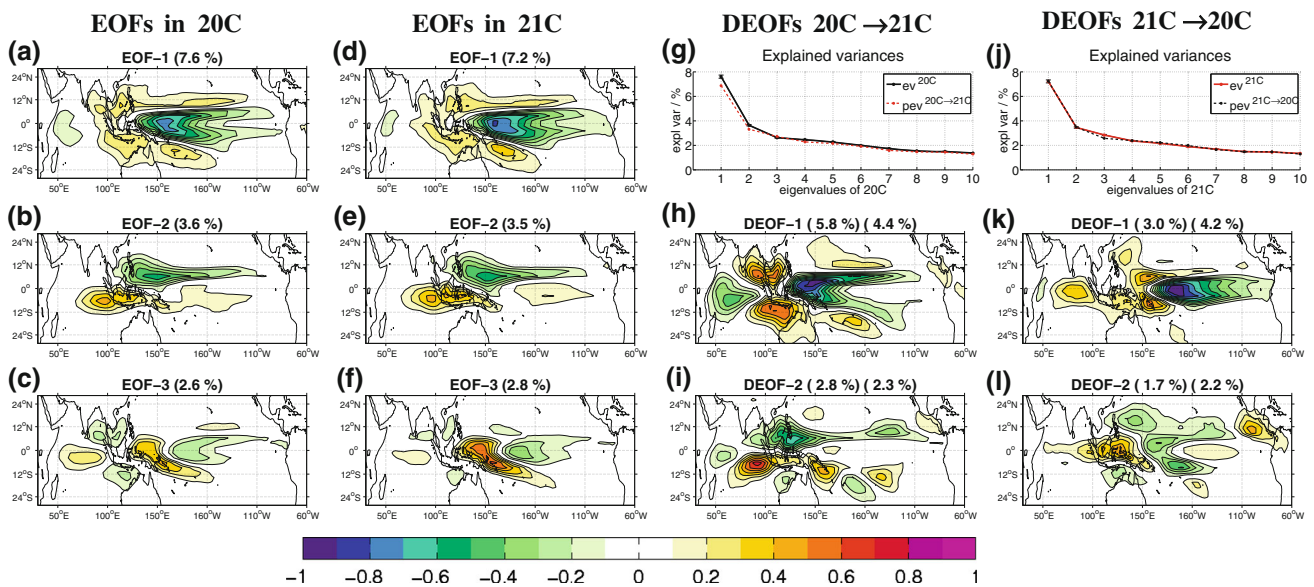
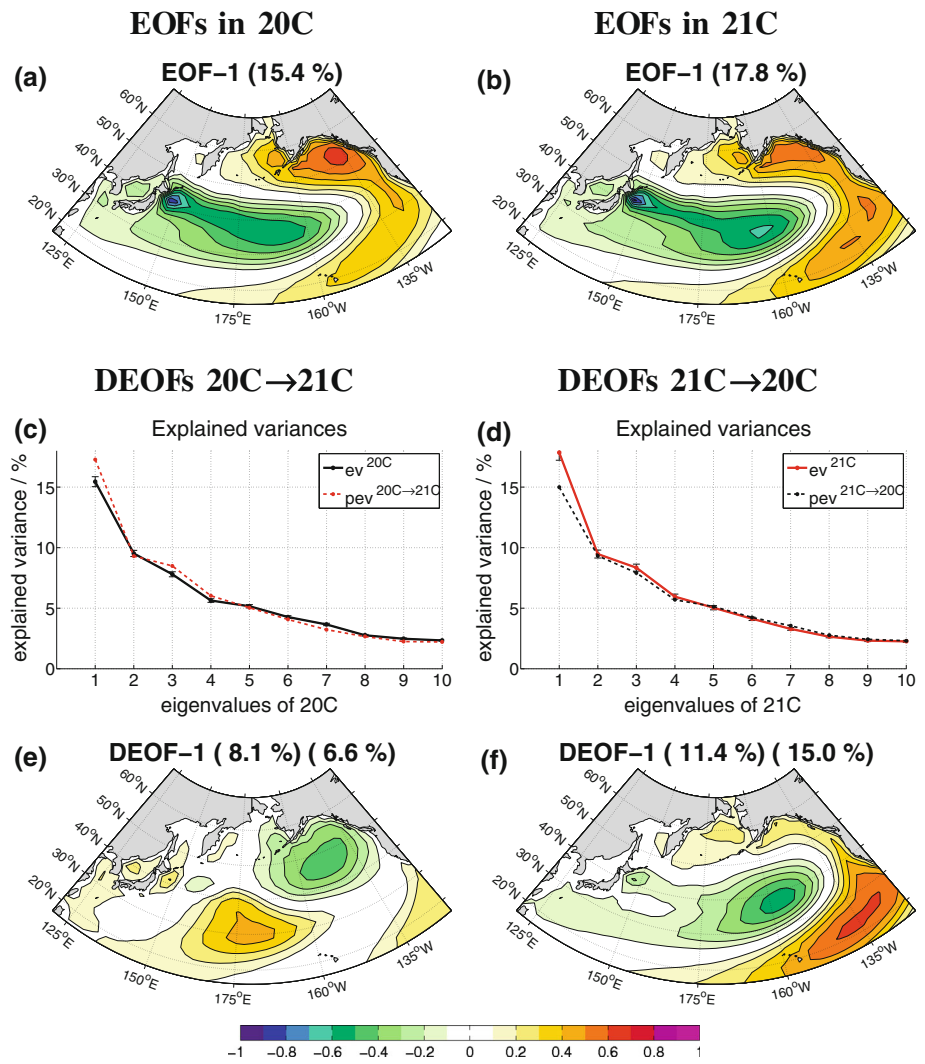


Fig. 14 Same as Fig. 9, but here for Tropical Indo-Pacific precipitation as discussed in Sect. 6.5

Table 4 DEOF-analysis recipe

Step	Comment
1. Define anomalies for both data sets	
2. EOF analysis for both data sets	Use identical domains and define eigenvalue variances in terms of relative explained variance [%]
3. Define the EOF-modes of one dataset as the reference modes	This defines the reference modes (patterns) on which you base your analysis
4. Project the reference EOF-modes onto the other dataset	This will allow you to compare the eigenvalue spectrum of the reference dataset with the projected explained variances of these modes in the other dataset
5. Compute the DEOF-modes by pairwise rotation to maximize the differences in explained variance of this mode in the two data sets	The DEOF-modes represent the modes in the reference dataset that have the largest difference in explained variance relative to the other dataset
6. Repeat steps 3–5 with the other dataset as the reference modes	If you first projected \mathcal{A} on \mathcal{B} , then now project \mathcal{B} on \mathcal{A}
7. Compare the results with idealized examples to understand the nature of the differences	The idealized examples will help you to formulate a simple model to describe the differences
8. Do further analysis to verify findings	No single statistical analysis will be sufficient. Use other statistical methods and, most importantly, sensitivity experiments or theoretical considerations to backup the results

increases by about 40 % relative to its value in the 20C simulations. Together with the DEOF-1^{20C→21C} (Fig. 14h), which is mostly the EOF-1 pattern losing relative importance in the 21C simulations, this illustrates an eastward shift of the ENSO related precipitation, in agreement with Chung and Power (2012). Both DEOF-2 (Fig. 14i, 1) also show significant changes that project on EOF-2 and show small-scale changes in the pattern shape. As all leading DEOF patterns are significant, this example illustrates that a multivariate system as a whole can change and it is not enough to look at the dominant mode only. But this example has also some similarity to the artificial example in Sect. 5.3 (shift in location). Here it is mostly an eastward shift in the dominant variability pattern.

7 Summary and discussion

In this study we introduced a method based on EOF analysis to quantify the differences in the modes of variability in two datasets, which is called DEOF analysis. It can be used to compare modes of variability in climate models with observations or find the changes in the modes of variability in climate change scenarios. We can summarize the DEOF analysis as a simplified recipe for the comparison of modes, see Table 4. The first feature of this method, the projected explained variances, reveals which EOF patterns are most distinct in two datasets. The second feature, the DEOF patterns, are the patterns with the largest differences in explained variance between two datasets and is also able to find small-scale changes in the modes of variability. The biggest advantage of this method is that it considers the changes in all patterns of variability instead of only the leading mode.

We further illustrated the method on the basis of several well-defined constructed examples. These examples do not only demonstrate the application of the DEOF method, but are also role models for formulating simple hypothesis for the differences in modes of variability between two datasets of real data analysis. Table 3 can basically be used as a look up table for the characteristics of the spatial variability differences. These characteristics are mainly: an intensification, a shift or a multivariate difference.

In the application of the DEOF analysis to literature examples we demonstrated that we could reproduce the main findings of the previous studies. Furthermore, we could also demonstrate that the DEOF analysis may in some aspects be more powerful than previously used methods. We detected the northeastward shift of the NAO pattern as in the paper from Hu and Wu (2004) and beyond that we could also find how much explained variance is gained and lost in certain regions. We could also find the pole-ward shift of the SAM with the DEOF method as described in Kidston and Gerber (2010), and beyond that we found that this is strongest over the Pacific Ocean. Further we investigated changes in the modes of Northern Hemispheric winter T_{surf} in global warming and found an eastward shift in the dominant mode, which is the manifestation of the NAO in T_{surf} . From the northeastward shift of NAO in SLP we expected this shift in the dominant mode of T_{surf} , which Keeley et al. (2008) could not find in a similar analysis. We think that their conclusion being different from ours is on the one hand based on the fact that they use only one model instead of a multi model ensemble to investigate the changes and on the other hand that their method (pattern correlation) aims on changes in the large scale pattern structure and while our method can also detect local changes in the patterns. For the modes of North

Pacific SST we could also find in contrast to Furtado et al. (2011) significant changes: A shift of the eastern part of the PDO and a strengthening in the southeastern part of the PDO. Furtado et al. (2011) did not made any statement about the method they used to compare the modes of variability, thus again we think their conclusion being different from ours is mostly based on the fact that their method aims more on the large scale changes in the modes of variability while our method can also detect local changes in the patterns. In the modes of precipitation we found an eastward shift in the ENSO related precipitation (EOF-1) in agreement with Chung and Power (2012), but beyond that also significant changes in the higher ordered modes, thus in the whole multivariate structure.

Finally, we need to note that although we think that the DEOF analysis method is a powerful new tool to help evaluate the differences in the spatial structure of climate variability, the interpretation of DEOF-modes or EOF-modes can be complicated (See e.g. Dommenget and Latif 2002). Alternative statistical methods, model sensitivity simulations and theoretical considerations of the climate processes involved should accompany any analysis of these complex multivariate datasets.

Acknowledgments We acknowledge the individual modeling groups, the Climate Model Intercomparison Project (CMIP3). This work was supported by the Deutsche Forschungsgemeinschaft (DFG) through project DO1038/5-1 and the ARC Centre of Excellence in Climate System Science (CE110001028). We thank Jan Harlaß, Klaus Getzlaff, Katja Lorbacher and Gang Wang for discussion and useful comments.

References

- Bretherton CS, Widmann M, Dymnikov VP, Wallace JM, Bladé I (1999) The effective number of spatial degrees of freedom of a time-varying field. *J Clim* 12:1990–2009
- Chung CTY, Power SB (2012) Nonlinear El Nino rainfall changes under global warming. Submitted to *Clim Dyn*
- Dommenget D (2007) Evaluating EOF modes against a stochastic null hypothesis. *Clim Dyn* 28:517–531
- Dommenget D, Latif M (2002) A cautionary note on the interpretation of EOFs. *J Clim* 15:216–225
- Furtado JC, Di Lorenzo E, Schneider N, Bond NA (2011) North Pacific decadal variability and climate change in the IPCC AR4 models. *J Clim* 24:3049–3067. doi:10.1175/2010JCLI3584.1
- Hu Z, Wu Z (2004) The intensification and shift of the annual North Atlantic Oscillation in a global warming scenario simulation. *Tellus A* 56A:112–124
- Hu Z-Z, Kumar A, Jha B, Huang B (2012) An analysis of forced and internal variability in a warmer climate in CCSM3. *J Clim* 25:2356–2373
- Hurrell JW, Van Loon H (1997) Decadal variations in climate associated with the North Atlantic Oscillation. *Clim Change* 36:301–326
- Jolliffe I (2002) *Principal component analysis*, 2nd edn. Springer, New York
- Keeley SPE, Collins M, Thorpe AJ (2008) Northern hemisphere winter atmospheric climate: modes of natural variability and climate change. *Clim Dyn* 31:195–211. doi:10.1007/s00382-007-0346-6
- Kidston J, Gerber EP (2010) Intermodel variability of the poleward shift of the austral jet stream in the CMIP3 integrations linked to biases in 20th century climatology. *Geophys Res Lett* 37:1–5. doi:10.1029/2010GL042873
- Krzanowski WJ (1979) Between-groups comparison of principal components. *J Am Stat Assoc* 74:703–707. doi:10.1080/01621459.1979.10481674
- Kuzmina SI (2005) The North Atlantic oscillation and greenhouse-gas forcing. *Geophys Res Lett* 32:1–4. doi:10.1029/2004GL021064
- McHugh MJ, Rogers JC (2005) Multi-model representation of the North Atlantic oscillation in the 20th and 21st centuries. *Geophys Res Lett* 32:1–4. doi:10.1029/2005GL023679
- Meehl GA, Covey C, Delworth T, Latif M, McAvaney B, Mitchell JFB, Stouffer RJ, Taylor KE (2007) THE WCRP CMIP3 multimodel dataset: a new era in climate change research. *Bull Am Meteorol Soc* 88:1383. doi:10.1175/BAMS-88-9-1383
- Miller RL, Schmidt GA, Shindell DT (2006) Forced annular variations in the 20th century intergovernmental panel on climate change fourth assessment report models. *J Geophys Res* 111:1–17. doi:10.1029/2005JD006323
- North GR, Bell TL, Cahalan RF (1982) Sampling errors in the estimation of empirical orthogonal functions. *Mon Weat Rev* 110:699–706
- Osborn TJ (2004) Simulating the winter North Atlantic oscillation: the roles of internal variability and greenhouse gas forcing. *Clim Dyn* 22:605–623. doi:10.1007/s00382-004-0405-1
- Petoukhov V, Semenov VA (2010) A link between reduced Barents-Kara sea ice and cold winter extremes over northern continents. *J Geophys Res* 115:D21111. doi:10.1029/2009JD013568
- Rauthe M, Hense A, Paeth H (2004) A model intercomparison study of climate change-signals in extratropical circulation. *Int J Climatol* 24:643–662
- Sengupta S, Boyle JS (1998) Using common principal components for comparing GCM simulations. *J Clim* 11:816–830. doi:10.1175/1520-0442(1998)011<0816:UCPCFC>2.0.CO;2
- Stephenson DB, Pavan V, Collins M, Junge MM, Quadrelli R (2006) North Atlantic Oscillation response to transient greenhouse gas forcing and the impact on European winter climate: a CMIP2 multi-model assessment. *Clim Dyn* 27:401–420. doi:10.1007/s00382-006-0140-x
- Wallace JM, Gutzler DS (1981) Teleconnections in the geopotential height field during the Northern Hemisphere winter. *Mon Weat Rev* 109:784–812